Spin-polarizing ^{3}He nuclei with an arc-lamp-pumped neodymium-doped lanthanum magnesium hexaluminate laser

Thomas R. Gentile and Robert D. McKeown
W. K. Kellogg Radiation Laboratory, California Institute of Technology, Pasadena, California 91125
(Received 22 June 1992)

We report a systematic study of optical pumping of ^{3}He nuclei by metastability exchange using an arc-lamp-pumped neodymium-doped lanthanum magnesium hexaluminate (Nd:LMA) laser. The laser produces 6 W at 1083 nm in a 1.5-GHz bandwidth and yields a substantial improvement in attainable nuclear polarization and pumping rates. Spin-polarized ^{3}He has applications in several fields of physics; the focus in this article is on targets for nuclear physics, which require high pumping rates to maintain the highest polarization. We have studied the influence of the ^{3}He pressure, pumping transition, discharge intensity and frequency, cell size and shape, and laser power on both the polarization and pumping rate. Under ideal conditions, we obtain 85% nuclear polarization. With pumping rates of 10^{18} (10^{19}) atoms/s, 82% (50%) polarization is obtained. We have found a pressure-dependent saturation of the increase in pumping rate with laser power. Based on our results, we discuss projections for the performance of both internal and external targets.

PACS number(s): 32.80.Bx, 29.25.Pj, 42.55.Rz

I. INTRODUCTION

The metastability exchange technique for spin-polarizing ^{3}He nuclei was demonstrated by Colegrove, Schearer, and Walters [1] nearly thirty years ago. However, the invention and continuing improvement of laser sources have increased the optical-pumping efficiency substantially [2–5]. We have obtained further improvements in the attainable polarization and pumping rate utilizing the recent developments in arc-lamp-pumped Nd:LMA lasers [6–9]. (Nd:LMA stands for neodymium-doped lanthanum magnesium hexaluminate and is also referred to as Nd:LNA, or just LNA.) The pumping rate, i.e., the rate at which ^{3}He nuclei can be polarized, is particularly important for the construction and optimization of targets for nuclear physics. In such targets, the highest polarization can only be maintained if the pumping rate is much higher than the relaxation rate in the target. Hence the focus of this article is on obtaining high polarization with high pumping rates. We have studied the influence of the ^{3}He pressure, pumping transition, discharge intensity and frequency, cell size and shape, and laser power, and the interaction of these parameters. The results constitute a large body of information that should be useful in any application of polarized ^{3}He nuclei.

Spin-polarized ^{3}He has applications in many areas of physics [9], including quantum statistics, polarized epithermal neutron beams [10], and polarized targets for nuclear physics experiments. In nuclear physics, polarized ^{3}He targets are interesting because the spin-dependent properties of the polarized ^{3}He nucleus are dominated by the neutron in the nucleus. Goals of current experiments using spin-polarized ^{3}He nuclei include measuring the electric and magnetic form factors of the neutron [11–13] and spin-dependent structure functions of the neutron [14]. The targets fall into two categories: external targets, which are closed systems, and internal targets, in which polarized gas is pumped away after exiting an open-ended target cell. An external polarized ^{3}He target constructed in our laboratory has recently been used successfully to study the quasielastic scattering of polarized electrons from polarized ^{3}He [11–13]. We have proposed future experiments at the Bates and Continuous Electron Beam Accelerator Facility (CEBAF) accelerators using targets of this type [15,16]. Eckert *et al.* [17] and Otten [18] have recently developed an external target utilizing compression to increase the density of the polarized gas. Internal targets are operated within storage rings to take advantage of the high luminosity available in these machines and to avoid scattering from the windows required in external targets. Recently, an internal polarized ^{3}He target [19,20] has been employed at the Indiana University Cyclotron Facility.

In both external and internal targets, the polarization must be maintained in the presence of significant relaxation mechanisms ($\sim 10^{17}$ atoms/s). For example, in an internal target the gas must be polarized faster than the flow rate out of the target cell. In external targets there is relaxation on the target walls and due to the particle beam. We have obtained pumping rates of $\gtrsim 10^{18}$ polarized atoms/s, which will allow the operation of polarized ^{3}He targets with minimal depletion of the polarization due to relaxation mechanisms. Based on these results, we present projections for the performance of both external and internal targets.

Because of the high photon energy (21 eV) required to reach the first excited state in ^{3}He, direct optical pumping, as done in alkali metals, is not practical with current laser technology. Instead an indirect approach is taken in which metastable ^{3}He atoms are polarized, and the polarization is transferred to the ground-state atoms in metastability exchange collisions. Metastable $2\,^3S_1$ atoms are produced by an electrodeless rf discharge in a glass cell filled to a pressure of ~ 1 torr of pure ^{3}He. The

 ©1993 The American Physical Society

metastables are optically pumped using the $2\,^3S_1 \rightarrow 2\,^3P_0$ transition at 1083 nm, and the resultant electronic polarization is partially transferred to the nuclei by the hyperfine interaction. In a metastability exchange collision, the incoming metastable atom transfers its atomic excitation to the incoming ground-state atom, leaving the outgoing ground-state atom with the partially polarized nucleus.

The indirect nature of the optical pumping of ^{3}He nuclei is rather complex to analyze in detail [21]. In addition, we do not have a detailed knowledge of the complex discharge environment. A number of interacting parameters affect the achievable polarization and pumping rate. In view of the obstacles to a full theoretical understanding over a wide range of conditions, we have taken the pragmatic approach of studying directly the quantities of greatest interest: the polarization and the pumping rate. In addition, we characterize the conditions of our measurements using easily measurable quantities that should be reproducible by others in the field.

In Sec. II we review the apparatus for optical pumping of ^{3}He, focusing on the Nd:LMA laser. In Sec. III we present results and systematics of optical pumping of ^{3}He with such a laser. Projections for targets are discussed in Sec. IV and we conclude the paper in Sec. V.

II. APPARATUS

A. Overview

A schematic diagram of the apparatus is shown in Fig. 1. Since we present results obtained by optical pumping of sealed cells only, the apparatus is rather simple. A cylindrical Pyrex ^{3}He cell is located at the center of an 80-cm-diameter Helmholtz coil (H), which provides a uniform magnetic field of 1.2 mT. A rf high voltage applied to two or four electrodes on the outside of the cell generates a weak electrical discharge in the ^{3}He gas. The circularly polarized laser light travels parallel to the magnetic field axis, hereafter referred to as the quantization axis. We determine the ^{3}He polarization by measuring the degree of circular polarization of the 668-nm ($3\,^1D_2 \rightarrow 2\,^1P_1$) light emitted from the discharge [22,23].

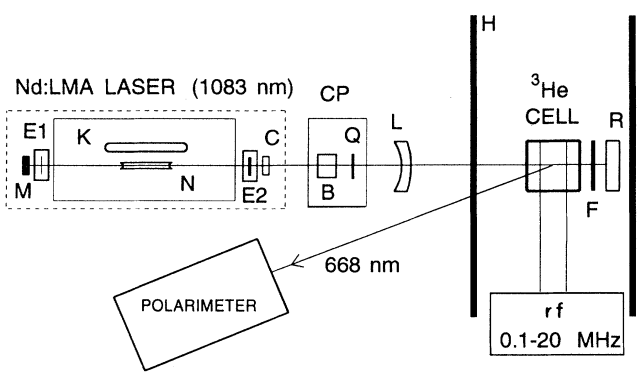

FIG. 1. Schematic diagram of the apparatus (not to scale). Laser elements: M, fully reflecting end mirror; $E1$, temperature-controlled 0.3-mm étalon; K, Kr arc lamp; N, Nd:LMA rod; $E2$, temperature-controlled 1.0-mm étalon; C, 99.0% reflecting output coupler. The solid line enclosing the lamp and rod shows the extent of the 28-cm-long laser head. (Within the dotted line surrounding the laser elements the drawing is roughly to scale along the optic axis.) Other elements: CP, circular polarizer, consisting of B, polarizing beamsplitter cube and Q, quarter-wave plate; L, weak diverging lens; H, Helmholtz coil; F, filter; R, retroreflector. The observation angle of the polarimeter with respect to the quantization axis has been exaggerated for clarity; the actual angle is 7°.

If the discharge is turned off, the dominant relaxation mechanism is due to gradients in the magnetic field. Gradients in magnetic field components transverse to the quantization axis relax the polarization because the moving atoms experience a randomly fluctuating magnetic field direction [24]. The gradients in our system resulted in relaxation times of 3500–6000 s for cells with pressure $\gtrsim 0.5$ torr. Since the relaxation time with the discharge on was between 10 and 1000 s, the relaxation time was dominated by the discharge. Although for lower pressures the relaxation time from gradients was as low as 1200 s, the relaxation time due to the discharge was always shorter than 250 s at these pressures.

B. The arc-lamp-pumped Nd:LMA laser

Although the arc-lamp-pumped Nd:LMA laser has been described elsewhere [6–9], we discuss the design and our own experience for completeness. The arc-lamp-pumped Nd:LMA laser has several properties that yield efficient optical pumping: high power (6 W), a linewidth well matched to the 2-GHz Doppler bandwidth of the ^{3}He gas, several longitudinal modes within this bandwidth, and good spectral overlap with the optical-pumping transition. In addition, the laser is simple to construct and easy to operate. No previous laser used for optical pumping of ^{3}He can claim all of these virtues. We use a Laser Applications Model 9560 cw Nd:YAG (where YAG denotes yttrium aluminum garnet) laser with some minor modifications: a Nd:LMA rod antireflection coated at 1083 nm replaces the Nd:YAG rod and two étalons are added to the laser cavity for tuning and bandwidth reduction. The configuration is very similar to that of Leduc [6,9]. The laser can be tuned by tilting the étalons or by varying their temperatures.

The most notable idiosyncracy of this laser is the lamp-current-dependent thermal lensing exhibited by the Nd:LMA crystal, which is caused by heating of the rod by the intense light from the arc lamp. Because the outside surfaces of the rod are water cooled a temperature gradient develops in the rod, which results in a gradient in the index of refraction. The rod acts like a converging lens with a focal length that shortens as the lamp current is increased. If the lamp power is sufficiently high to cause a focus within the laser cavity, the laser power drops and the user risks the crystal's demise from thermal stress. Before this disaster occurs, there are warning signs: the beam shape of the laser begins to deteriorate, the laser requires realignment to maximize the power, and the increase of the laser power with lamp current saturates. To alleviate the effects of thermal lensing, we use a short cavity and rod ends with concave

(R =45 or 60 cm) curvature. The cavity is 36 cm long, but 28 cm is occupied by the commercial laser head that houses the rod and lamp. We have also operated the laser with flat ends, but obtain a more uniform spatial profile of the beam at high power using curved ends. The better beam shape facilitates uniform coverage of the ^{3}He cell, minimizes saturation of the pumping transition, and empirically leads to more efficient optical pumping. For a curvature of 60 (45) cm the threshold lamp power of the laser is increased by a factor of 1.6 (2.0) above that obtained with flat ends because at low lamp current the curvature overcompensates the thermal lensing. As the lamp current is increased the power output using curved rods quickly reaches and ultimately surpasses the output using flat ends. For 60- (45-) cm curvature, typical operating parameters for the lamp power are 1.0 (1.2) kW for the laser threshold and 1.8 kW (2.1 kW) for 6 W output.

The 4-mm-diameter by 79-mm-long Nd:LMA rod (N), grown along the a axis and doped with $\approx 15\%$ Nd, was purchased from Union Carbide. Because of the asymmetry in the thermal conductivity along the b and c axes [6], typically the beam shape is elliptical. The ellipiticity increases with lamp current and seems to vary from rod to rod. The recent development of rods grown along the c axis [25] should have more cylindrically symmetric thermal properties and hence less elliptical beam shapes.

The light is coupled out of one end of the laser using a partially reflecting mirror (C). We have tested output couplers with 98.2%, 99.0%, and 99.4% reflectivity and find that the 99.0% coupler yields a factor of 2 (1.3) higher output power than that obtained with 98.2% (99.4%). We obtain the highest laser power with the mirrors located symmetrically about the Nd:LMA rod.

To tune the laser and reduce the linewidth, two uncoated étalons, one 0.3 mm thick ($E1$) and the other 1.0 mm thick ($E2$), are added to the laser cavity. This configuration yields a 1.5-GHz linewidth. Using two étalons yields a narrower linewidth, higher pumping rates, and more reliable operation than using a single étalon. A single 0.3-mm étalon does not yield good resolution of the 6.7-GHz hyperfine splitting in the $2\,^3S_1$ state. Although the linewidth is improved using a single 0.75- or 1.0-mm étalon, the pumping rates are still inferior to those obtained with two étalons [26]. Since the free spectral range at these thicknesses is smaller than the fluorescence bandwidth of the laser, the root of the inferior performance may be that two different wavelengths are competing for gain.

Although the laser can be tuned by tilting the étalons, this approach is not ideal. As an étalon is tilted away from normal incidence, the reflected waves from the two faces of the étalon interfere less efficiently, resulting in a drop in power. In addition, the beam shape degrades with increasing tilt angle. To eliminate this problem, we have followed the approach of Larat [27] by positioning the étalons near normal incidence and varying their temperatures for tuning. This has an added advantage because the dominant source of frequency drift of the laser is eliminated when the temperature of the étalons are stabilized. The étalon heater is a homemade system consisting of a copper block that surrounds the étalon, a resistive wire heater, and a feedback circuit to regulate the temperature. The heater is 2.5 cm long and rests on a 3.5-cm-diameter rotation stage (Ealing Electro-Optics Model 37-0502), allowing the end mirrors of the laser to be only 4 cm from the laser head.

To circularly polarize the laser light we use a linearly polarizing beamsplitter cube (B) followed by a multiple-order quartz quarter-wave plate (Q). These two components are assembled as a unit (CP) which is also used an an attenuator by rotating the unit around the propagation direction of the light. (This arrangement functions as an attenuator because the light emerges from the laser linearly polarized.) A small deviation from perfectly circularly polarized light can decrease the maximum obtainable polarization [17,27]. We measured the degree of circular polarization of the laser light to be 99.7% by analyzing it with a second beamsplitter cube. Based on the calculations of Larat [27], we might be able to improve some of our polarization results slightly ($\sim 2\%$) by using a higher degree of circular polarization, mainly when the C_9 pumping transition is used (the nomenclature for the pumping transitions can be found in Sec. III).

For the 3.3-m distance from the laser to the cell (chosen for convenience), the divergence of the beam is not quite sufficient to illuminate the cell uniformly. For cells of 4.7 (7.0) cm inside diameter (i.d.), we expand the beam with a weak diverging lens (L) of focal length -4000 (-1000) mm located 1.4 m from the cell. This was adequate, but a parallel, expanded beam would be preferable, especially for longer cells. For all the results discussed in this paper (except results versus laser power) the laser power P_L incident on the cells was 4.5 W. This required an actual output power of 5.5 W because of losses from two mirrors (not shown in Fig. 1), the circular polarizer assembly, and the uncoated lens.

For maximum optical-pumping efficiency it is desirable to interact with the entire velocity profile of the metastable atoms. The number of velocity groups that interact with the laser light is doubled by using a retroreflector (R) after the cell. To avoid reflection of the 668-nm light used for polarization measurement a filter (F) that absorbs this wavelength but transmits the laser light (CVI Laser Corp. RG850 or Kodak Wratten 87B) is placed before the retroreflector.

C. Polarization measurement

For a system of spin-$\frac{1}{2}$ particles, the nuclear polarization is defined as

$$P \equiv \frac{n_+ - n_-}{n_+ + n_-} , \tag{1}$$

where n_+ and n_- are the number densities for the two eigenstates of the spin with respect to the quantization axis. Because of the hyperfine interaction, the degree of circular polarization of the 668-nm light emitted from the discharge is proportional to the nuclear polarization. When ^{3}He atoms are excited to the $3\,^1D_2$ level by electron impact in the discharge, the nuclear spin is unperturbed. During the 15-ns lifetime of the $3\,^1D_2$ state, the

TABLE I. Comparison of the calibrations of the optical method for measuring nuclear polarization in ^{3}He. The calibration factor is the ratio of the nuclear polarization to the degree of circular polarization of the 668-nm light. The nuclear polarizations reported in this paper were determined using the fitted dependence of the calibration factor on pressure in Ref. [29].

	Calibration factor	
Pressure	Ref. [29]	Ref. [28]
0.10	5.67	
0.20	6.41	7.3
0.30	6.75	7.5
0.49	7.31	8.0
0.78	7.98	8.7
1.0	8.41	9.3
2.0	10.01	11.6
2.9	11.42	13.8
4.9	14.98	17.8

nuclear polarization is mixed into electronic polarization by the hyperfine interaction. As a result of this mixing, the subsequent spontaneous emission shows some degree of circular polarization which can be related to the nuclear polarization. However, some of the electronic polarization is lost due to collisions, hence this relationship depends on pressure and requires calibration. In a series of NMR measurements, we have recently improved the long-standing calibration of this method [28]. In addition, we have carefully analyzed the systematics of the optical method itself. A full description of these results is reported in the following paper [29]. As we have incorporated this new calibration into the results reported in this paper, in Table I we compare the new calibration of Ref. [29] to the old calibration in Ref. [28]. In all cases the new calibration yields lower polarization values.

III. OPTICAL-PUMPING RESULTS AND SYSTEMATICS

In the following discussion, we consider the influence and interaction of several parameters that are relevant to optical pumping of ^{3}He. These include the ^{3}He pressure, the intensity and frequency of the electrical discharge, the pumping transition, the laser power, and the size and shape of the ^{3}He cell. The most dramatic changes in the pumping rate arise from increasing the discharge intensity, but at the expense of polarization. Higher discharge levels increase the metastable density, hence the pumping rate, but also generate more relaxation in the coupled metastable–ground-state system. We have chosen to characterize the discharge intensity by the relaxation time τ_r of the nuclear polarization. Although other parameters are certainly important, most notably the metastable density, we chose the relaxation time because it is easily measurable and reproducible. (As mentioned earlier, the relaxation time is usually dominated by the discharge, except for very long relaxation times, where magnetic field gradients and ultimately surface characteristics become relevant.)

The two transitions that are most useful for optical pumping are the $2\,^3S_1\,F=\frac{3}{2}\rightarrow 2\,^3P_0\,F=\frac{1}{2}$ and $2\,^3S_1\,F=\frac{1}{2}\rightarrow 2\,^3P_0\,F=\frac{1}{2}$ transitions, conventionally labeled C_8 and C_9, respectively. The frequency difference between these transitions of 6.7 GHz is easily resolved by the laser.

A. Polarization versus pressure

The dependence of the polarization on pressure is shown in Fig. 2 for three discharge intensities. The highest polarization observed is 84% at 0.8 torr. Until the advent of the arc-lamp-pumped Nd:LMA laser, the highest polarization that had been observed was 65% (using the new calibration data in Table I.) Unfortunately, the polarization declines with increasing pressure above 0.3 torr. For strong discharges the decline in the polarization with pressure is steeper than for weak discharges. Some data points are missing because it is difficult to maintain very weak discharges at low pressure. Although several ideas have been proposed for the decline of polarization with increasing pressure, it is not understood in detail.

B. Temporal behavior of the optical pumping

Before discussing our studies of the pumping rate, we need to define this term more precisely. The simplest differential equation to model the dynamics of the optical pumping is

$$\frac{dP(t)}{dt}=\frac{[P_m-P(t)]}{\tau_p}-\frac{P(t)}{\tau_r}\ , \tag{2}$$

where $P(t)$ is the instantaneous polarization, P_m is the maximum polarization for $\tau_r\rightarrow\infty$, and τ_p and τ_r are the

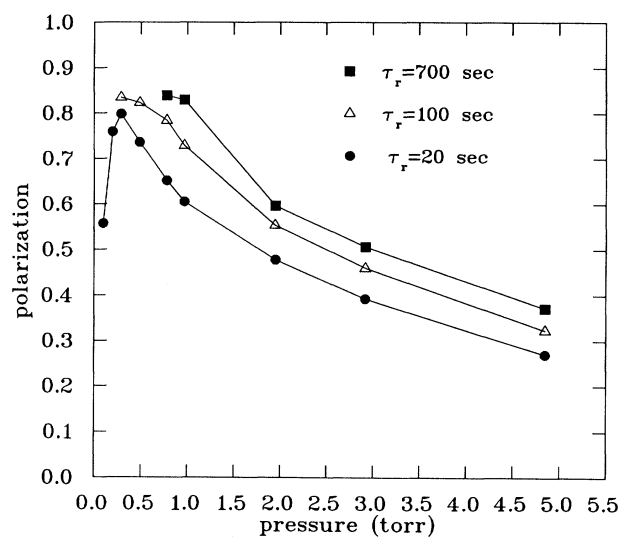

FIG. 2. Nuclear polarization vs pressure for 4.7-cm-i.d. by 5.4-cm-long, 90-cm^3 cells, shown for three discharge intensities. The pumping transition and discharge frequency were chosen for each combination of pressure and discharge intensity to maximize the polarization, regardless of pumping rate. The conditions are C_8 for 0.1–1.0 torr, except C_9 for 1.0 torr ($\tau_r=20$ s only); C_9 for 2–5 torr; $\nu_d=10$ MHz for 0.1–0.3 torr, 1 MHz for 0.5 torr, 0.1 MHz for 1–5 torr; $P_L=4.5$ W.

pumping and relaxation time constants, respectively. If τ_p and τ_r are constant in time, the solution of Eq. (2) is a simple exponential:

$$P(t)=P_0[1-\exp(-t/\tau)] , \tag{3}$$

where

$$P_0=\frac{P_m}{1+(\tau_p/\tau_r)} \tag{3a}$$

is the final polarization and

$$\tau=\frac{\tau_p}{1+(\tau_p/\tau_r)} \tag{3b}$$

is an effective pumping time constant. A detailed numerical study of the dynamics of the optical pumping [27] reveals that τ_p^{-1} is not constant, but rather decreases as the polarization rises, and that this decrease is nearly linear in the regime of our interest. The results of a numerical calculation of the variation of τ_p^{-1} with polarization are shown in Fig. 3. The cause of the decrease in τ_p^{-1} is the decreasing absorption of the laser light as the metastable population shifts to magnetic sublevels that no longer interact with the light. To measure the dependence of τ_p^{-1} on polarization, we performed a simple experiment in our NMR system. (See Ref. [29] for a description of this system.) By inducing transitions between the two magnetic sublevels of the ground state with a rf magnetic field at the Larmor frequency, we shortened the relaxation time constant without changing the discharge characteristics that affect the pumping time constant. Using Eq. (3a), we obtain

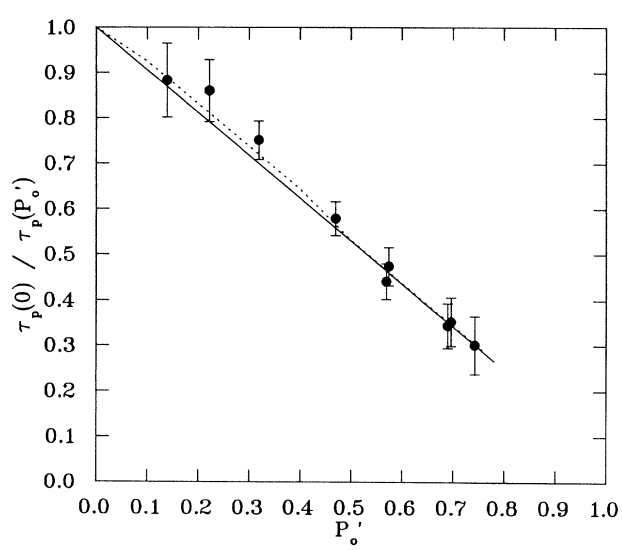

FIG. 3. Variation of $\tau_p(0)/\tau_p(P_0')$ with P_0' (see Sec. III B). The solid circles are the values obtained from measurements of P_0' and τ_r' using the procedure described in the text. The data were acquired with a 1.0-torr cell, $P_L=4$ W (tuned to the C_8 transition), $\tau_r=226$ s, and $P_0=0.770$. The dotted line is a numerical calculation [M. Leduc (private communication); similar calculations can be found in Ref. [27]] for similar conditions (0.8 torr, $P_L=3$ W, and $\tau_r=120$ s). The solid line is a linear approximation using the fitted value of m.

$$\tau_p^{-1}(P_0')=\frac{1}{\tau_r'}\left[\frac{P_0}{P_0'}\left[1+\frac{\tau_p(P_0)}{\tau_r}\right]-1\right]^{-1} , \tag{4}$$

where $\tau_p(P_0')$ $[\tau_p(P_0)]$ is the pumping time constant at polarization P_0' (P_0), P_0' (P_0) is the maximum polarization with the rf on (off), and τ_r' (τ_r) is the relaxation time constant with the rf on (off). We measured τ_r' as a function of P_0'. Although P_0 and τ_r were also measured, we cannot explicitly evaluate $\tau_p^{-1}(P_0')$ because $\tau_p(P_0)$ is not known. However, we can make a comparison to the numerical calculations in Fig. 3 using a two-step approach. First, we replace $\tau_p^{-1}(P_0')$ in Eq. (4) by a linear approximation, given by

$$\tau_p^{-1}(P_0')=\tau_p^{-1}(0)+mP_0' , \tag{4'}$$

where m is the slope of the line and $\tau_p^{-1}(0)$ is the intercept. Then we invert Eq. (4) to obtain τ_r' as a function of P_0'. The data are fit with $\tau_p^{-1}(0)$, m, and $\tau_p(P_0)$ as adjustable parameters. Values for $\tau_p^{-1}(P_0')$ are then determined for each combination of τ_r' and P_0' using the fitted value of $\tau_p(P_0)$ in Eq. (4). In this way the fitting is performed on the raw data and $\tau_p^{-1}(P_0')$ is evaluated from the results of the fit. If m and $\tau_p^{-1}(P_0)$ are normalized to $\tau_p(0)$, we obtain $m\tau_p(0)=0.94\pm0.19$ and $\tau_p(0)/\tau_p(P_0)=0.30\pm0.08$. Figure 3 shows the comparison between the values of $\tau_p(0)/\tau_p(P_0')$ and the numerical calculation. The agreement is good. The linear approximation is also shown for reference.

In Secs. III C–III E, we present studies of the pumping rate for a variety of conditions. For such studies it is convenient to have a single, easily measurable parameter to describe the pumping rate, despite the behavior discussed above. A simple exponential fit [Eq. (3)] to a typical pumping curve is shown in Fig. 4. There is a sys-

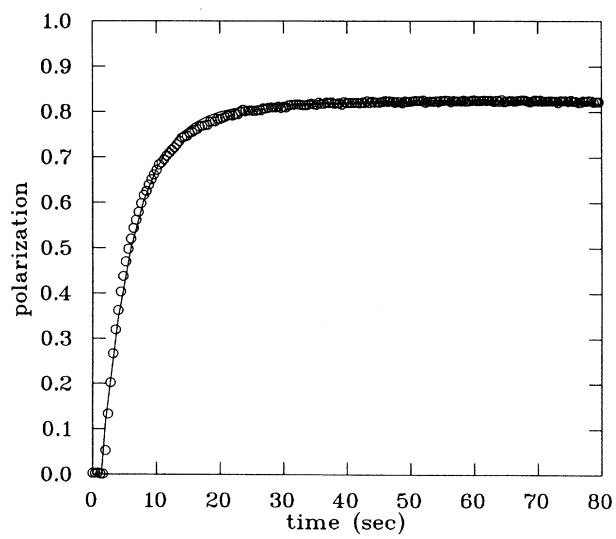

FIG. 4. Nuclear polarization vs time for a 0.3-torr, 7.0-cm-i.d. by 15-cm-long, 600-cm^3 cell. The solid line is a fit to $P(t)=P_0[1-\exp(-t/\tau)]$. The deviation of the data from the fit is discussed in the text. The conditions are $P_L=4.5$ W, $\nu_d=10$ MHz, and $\tau_r=84$ s.

tematic deviation of the data from the fit that is consistent with a pumping rate that declines with increasing polarization, as described above. Nevertheless, the time constant of the exponential is representative to the time scale of the buildup of polarization. Hence for convenience we define the pumping rate to be $R_p \equiv NP_0/\tau$, where P_0 and τ are the values extracted from a fit of the pumping curve to Eq. (3) and N is the number of atoms in the cell . (We took the precaution of fitting the data over the same range, typically at least ten times longer than the pumping time constant.) However, in Sec. IV, where the absolute value of the pumping rate at the polarization maintained in the target is relevant, the effect shown in Fig. 3 is taken into account.

C. Effects of pumping transition and discharge characteristics

We have chosen three pressures for more detailed results: 0.3, 1.0, and 2.0 torr. Changes occur in the optical-pumping characteristics over this range and as we will discuss later, these pressures are relevant for targets. Each cell for these three pressures is 7.0 cm i.d. by 15 cm long, yielding a volume of 600 cm^3. For each pressure we display the dependence of the polarization and the pumping rate on the discharge intensity. In addition, we combine this information into a single plot of polarization versus pumping rate. These plots succinctly summarize the results most relevant to target design.

We investigated the effect of the discharge frequency ν_d in the range 0.1–20 MHz and found that the choice of frequency has a significant effect on both the polarization and the pumping rate. While for a given discharge intensity, higher discharge frequency almost always yields a higher pumping rate, the effect on the polarization depends on the pressure. We display data for $\nu_d = 0.1$, 1, and 10 MHz—little change in either polarization or pumping rate was observed for discharge frequencies above 5–10 MHz. We do not show all frequencies for all pressures because the lower frequencies only show comparable or superior performance at the higher pressures. Although exactly how the choice of frequency affects the discharge is not understood, it is reasonable to assume that higher metastable densities result from higher discharge frequencies.

1. Results at 0.3 torr

At 0.3 torr the best polarization and pumping rate are obtained by using the highest discharge frequency. Figure 5 shows the dependence of the polarization and the pumping rate on the discharge intensity for $\nu_d = 10$ MHz. As the discharge intensity is increased, a dramatic improvement in the pumping rate is obtained with some decline in the polarization. Higher polarization is obtained using the C_8 transition, while higher pumping rate is obtained using the C_9 transition. At this pressure, the longest relaxation time corresponds to the weakest discharge that could be maintained in the cell. We arbitrarily did not go shorter than a relaxation time of ~ 10 s.

The data in Fig. 5 are combined into a single plot of polarization versus pumping rate, shown in Fig. 6. For the weakest discharge ($\tau_r = 230$ s) and pumping on the C_8 transition we obtained 85% polarization with a pumping rate of 4×10^{17} atoms/s, while for the strongest discharge tested ($\tau_r = 14$ s) and pumping on the C_9 transition, 67% polarization with a pumping rate of 4.7×10^{18} atoms/s was obtained.

2. Results at 1.0 torr

Figures 7 and 8 show similar plots for a pressure of 1.0 torr. Here we have added data taken with a discharge frequency of 1 MHz. For a given discharge intensity the polarization obtained using $\nu_d = 10$ MHz is lower than that obtained at 1 MHz, but the pumping rate is higher. The plot of polarization versus pumping rate reveals that the 10 MHz is the better overall choice, except perhaps at the lowest pumping rates. However, the ability to maintain a weak discharge depends on the pressure and the

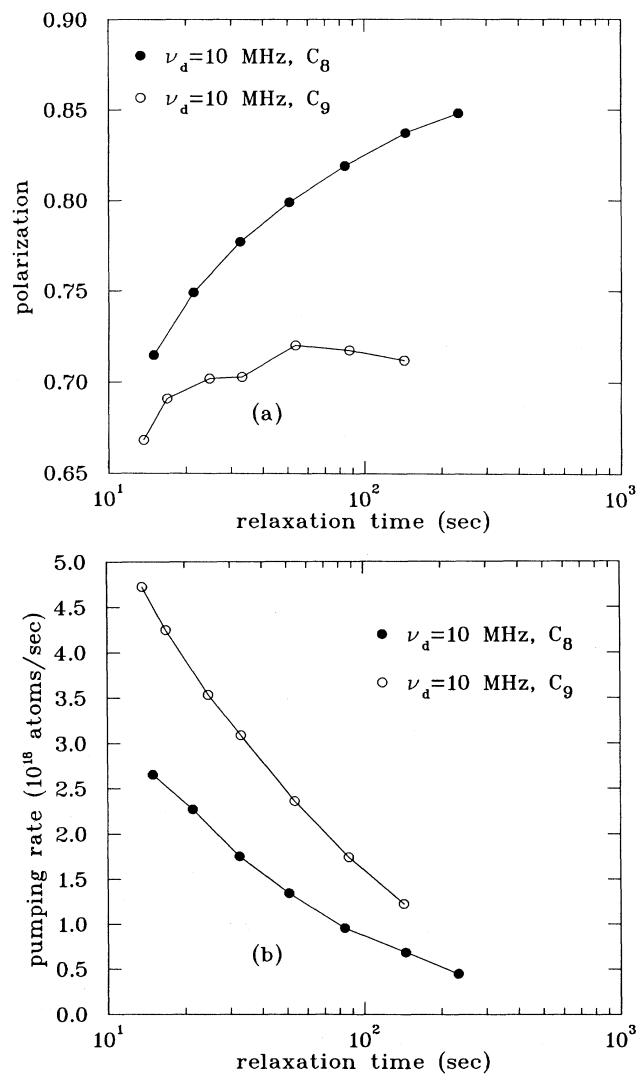

FIG. 5. Nuclear polarization (a) and pumping rate (b) vs discharge intensity for a 0.3-torr, 7.0-cm-i.d. by 15-cm-long, 600-cm^3 cell and $P_L = 4.5$ W.

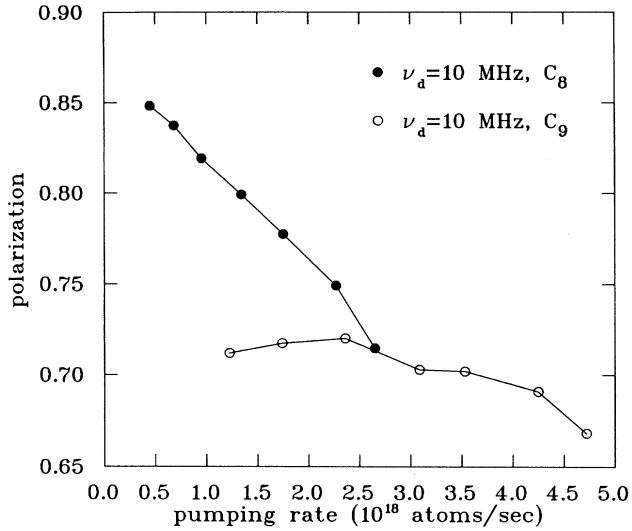

FIG. 6. Data from Fig. 5 combined into a plot showing nuclear polarization vs pumping rate for a 0.3-torr, 600-cm^3 cell.

cell geometry and is often more difficult at higher frequencies. Hence, for a different size cell, it may be impossible to obtain the highest polarizations using 10 MHz simply because the discharge will extinguish before it can be made weak enough.

The dependence on the pumping transition is similar to that at 0.3 torr, except that at high discharge intensities the C_9 transition yields higher polarization. For the weakest discharge ($\tau_r = 900$ s) tested and pumping on the C_8 transition we obtained 78% polarization with a pumping rate of 8×10^{17} atoms/s, while for the strongest discharge tested ($\tau_r = 15$ s) and pumping on the C_9 transition, 45% polarization with a pumping rate of 9×10^{18} atoms/s was obtained.

3. *Results at 2.0 torr*

Figures 9 and 10 show data obtained at 2.0 torr. At this pressure, pumping on the C_9 transition always yields higher polarization and pumping rate than for the C_8, hence to present uncluttered graphs we do not show results using C_8. The C_9 transition may yield superior performance because for this transition, the optical-pumping efficiency is least sensitive to mixing among the magnetic sublevels in the $2\,^3P$ state [21]. (This mixing increases at higher pressure.)

At 2.0 torr we obtain the highest polarization with a discharge frequency of 0.1 MHz, although it is only marginally better than that obtained with 1 MHz. From Fig. 10 we see that 1 MHz is preferable for low pumping rates, while 10 MHz is preferable at high pumping rates. Although low discharge levels could not be tested using 10 MHz because the discharge extinguished, the trend of the data suggested that 1 MHz would still be the preferable choice. A discharge frequency of 0.1 MHz is only desirable for the lowest pumping rates.

For the weakest discharge ($\tau_r = 900$ s) we obtained 57% polarization with a pumping rate of 1.1×10^{18} atoms/s, while for the strongest discharge ($\tau_r = 15$ s) 33% polarization with a pumping rate of 8.0×10^{18} atoms/s was obtained.

4. *Summary of effects of pumping transition and discharge characteristics*

Although specific conclusions depend on the size of the cell, laser power, etc., we can make some general observations: If we consider both pumping transitions, C_8 and C_9, increasing the discharge intensity yields an order-of-magnitude improvement in the pumping rate, but accompanied by a 20% loss in polarization at 0.3 torr and a 40% loss at 1 or 2 torr. For low pressures and weak discharges, the C_8 transition is preferable, while for high pressures and strong discharges, C_9 is preferable.

The discharge frequency has a significant effect on the optical-pumping efficiency. At low pressure ($\lesssim 1$ torr) or for strong discharges at any pressure, a high discharge

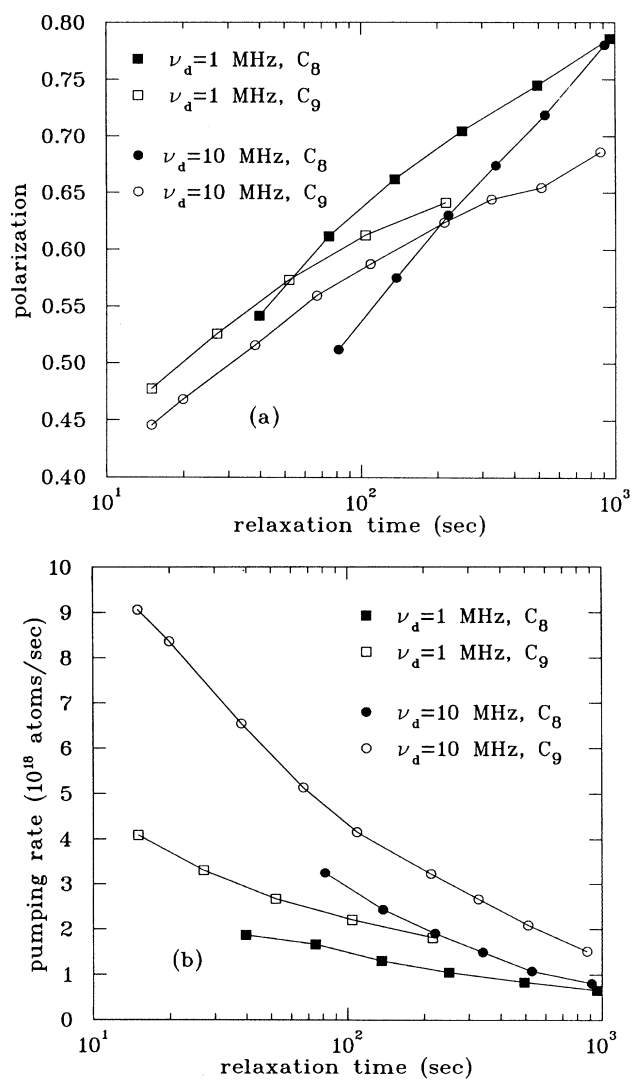

FIG. 7. Nuclear polarization (a) and pumping rate (b) vs discharge intensity for a 1.0-torr, 7.0-cm-i.d. by 15-cm-long, 600-cm^3 cell and $P_L = 4.5$ W.

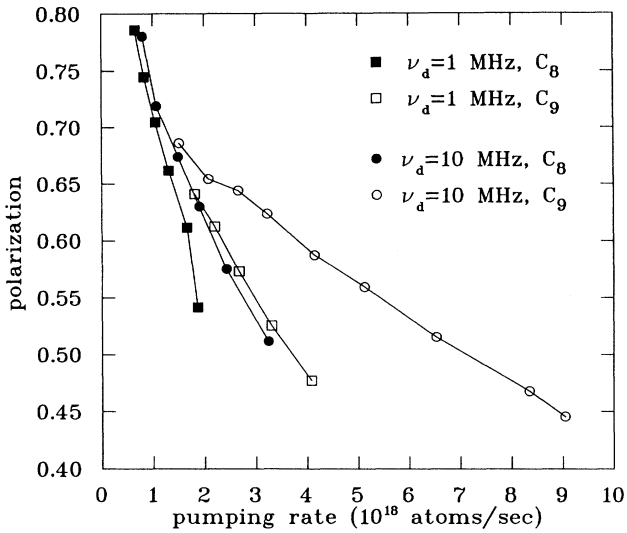

FIG. 8. Data from Fig. 7 combined into a plot showing nuclear polarization vs pumping rate for a 1.0 torr, 600-cm^3 cell.

frequency yields the highest polarization for a given pumping rate. For higher pressures and weak discharges, lower discharge frequencies yield comparable or superior performance. In some cases this may be simply because a weaker discharge can be maintained at lower frequencies.

D. Polarization and pumping rate versus laser intensity

Figure 11 shows the dependence of the polarization on laser power for a 0.3-torr, 7.0-cm-i.d. cell. In the regime of laser power now available the curve shows an extremely saturated form. For a numerical analysis of this form, we refer the reader to Ref. [21]. Similar plots are obtained at 1 and 2 torr.

Figure 12 shows the dependence of the pumping rate on laser power for 4.7-cm-i.d., 90-cm^3 cells at pressures of 0.3, 0.8, 3.0, and 5.0 torr. Each curve has been fit to the form

$$R=\frac{R_0}{1+(S/P_L)}\ , \tag{5}$$

where P_L is the laser power, and R_0 and S are adjustable parameters. To allow comparison of the shape of the curves, R/R_0 is plotted on the y axis. This simple saturation expression fits the data well and allows the extraction of a saturation parameter S. (However, we do not have a rigorous justification for this form.) The dependence of S on pressure for both the C_8 and C_9 transitions is shown in Fig. 13. For these small cells and weak discharges, the absorption of the laser light in the cell is minimal, hence the intensity is fairly uniform throughout the cell. A detailed analysis of the dynamics of the optical-pumping process would be required to fully understand the data in Fig. 13. Such an analysis would consider the absorption of the multimode laser, including the effects of collision and power broadening and the spatial and spectral characteristics of the laser. We have not carried out such an analysis, but offer the following interpretation for the general trends in these data. At low laser power the absorption rate R_a of pumping light by the metastables, hence the pumping rate, increases linearly with the laser power. We expect saturation of the pumping rate when R_a becomes comparable to the metastability exchange rate R_e. Since the metastability exchange rate increases linearly with the pressure, we expect that the saturation intensity would also increase linearly with the pressure. For the data taken at pressures at or below 1.0 torr, we observe a linear dependence of S on the pressure, as shown in Fig. 13. (In addition, a rough estimate of R_a at the saturation intensity is comparable to R_e.) At pressure above about 2 torr, the metastability exchange rate exceeds the spontaneous emission rate ($A=1\times10^7\ \mathrm{s}^{-1}$). In this case, we expect that saturation will occur when the absorption rate is comparable to the spontaneous emission rate. Thus at higher pressure, S should become independent of the pressure. We do observe this trend in the data in Fig. 13, but the dip in S at 3 torr is not understood.

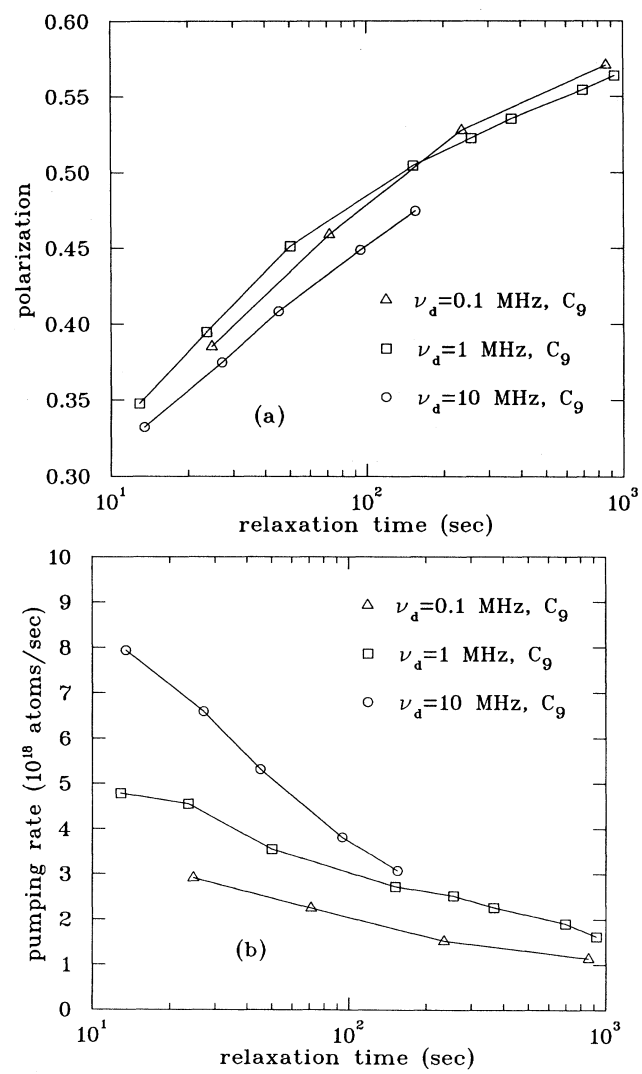

FIG. 9. Nuclear polarization (a) and pumping rate (b) vs discharge intensity for a 2.0-torr, 7.0-cm-i.d. by 15-cm-long, 600-cm^3 cell and $P_L=4.5$ W.

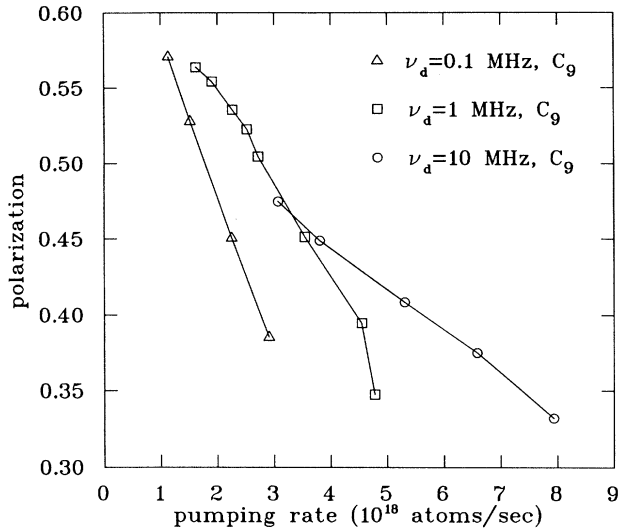

FIG. 10. Data from Fig. 9 combined into a plot showing nuclear polarization vs pumping rate for a 2.0-torr, 600-cm^3 cell.

We can compare the slopes of the linear fits of S versus pressure for the two pumping transitions. The ratio of slopes for the two transitions should be given by the reciprocal of the ratio of their respective oscillator strengths. However, a precise comparison is difficult because the C_9 transition has two relevant oscillator strengths a and b, corresponding to the $2\,^3S_1\,F=\frac{3}{2}$, $m_F=-\frac{3}{2}\rightarrow 2\,^3P_0\,F=\frac{1}{2}$, $m_F=-\frac{1}{2}$, and $2\,^3S_1\,F=\frac{3}{2}$, $m_F=-\frac{1}{2}\rightarrow 2\,^3P_0\,F=\frac{1}{2}$, $m_F=\frac{1}{2}$ transitions, respectively. The relative weighting of the two oscillator strengths depends on the relative populations of the $m_F=-\frac{3}{2}$ and $-\frac{1}{2}$ sublevels of the $2\,^3S_1$ state and hence on the polarization. For a rough estimate we choose half the maximum polarization and use the population distribution obtained

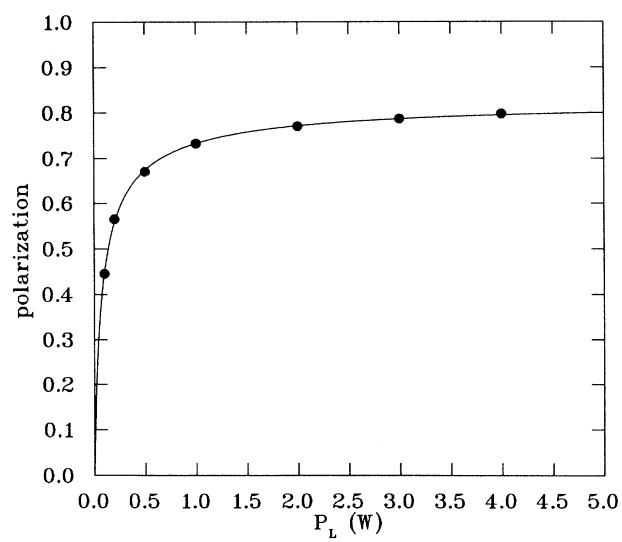

FIG. 11. Nuclear polarization vs laser power for a 0.3-torr, 7.0-cm-i.d. by 15-cm-long, 600-cm^3 cell. The beam area was ≈ 26 cm^2. The line is drawn to guide the eye. The conditions are laser tuned to C_8, $\nu_d=10$ MHz, and $\tau_r=39$ s.

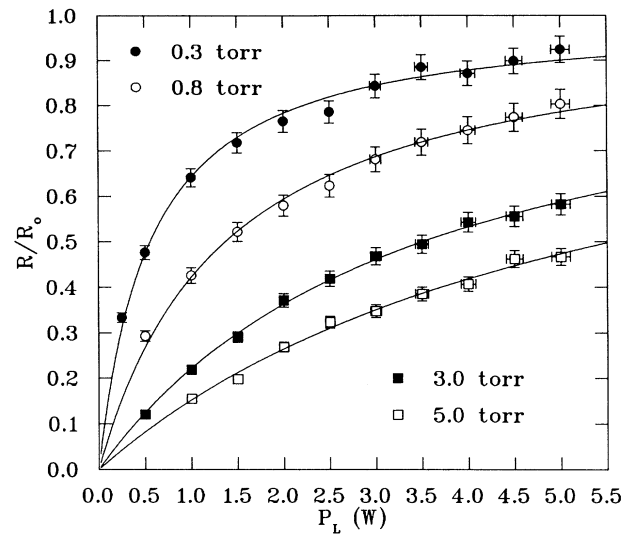

FIG. 12. R/R_0 (see Sec. III D) vs P_L for four pressures, obtained with 4.7-cm-i.d., by 5.4-cm-long, 90-cm^3 cells. The lines are fits of the data to the form discussed in the text. The conditions are laser tuned to C_8, $\nu_d=1$ MHz, and $\tau_r=300-350$ s, except for 0.3 torr, where $\tau_r=90$ s.

from spin temperature equilibrium [1,17,30]. If we define the oscillator strength for the C_8 transition to be unity, then the average oscillator strength for the C_9 transition and hence the ratio of slopes r is given by

$$r=\frac{M(C_8)}{M(C_9)}=\frac{1-P}{2}\left[a+b\frac{1+(P_0/2)}{1-(P_0/2)}\right], \tag{6}$$

where $M(C_8)$ and $M(C_9)$ are the slopes for C_8 and C_9, respectively, P_0 is the maximum polarization, $a=0.96$, and $b=0.32$ (Ref. [21]). For the C_9 data in Fig. 13 between 0.3 and 1.0 torr, P_0 is typically 0.75. This yields a ratio of slopes of $r=0.52$, which is consistent with the observed ratio of 0.55.

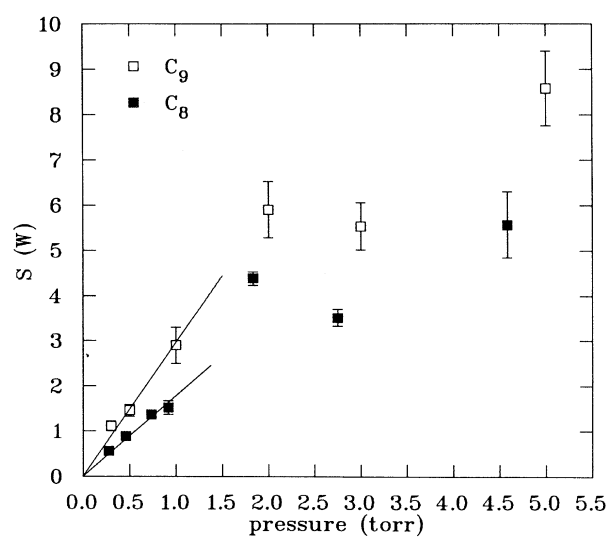

FIG. 13. The saturation parameter S vs pressure, obtained from the fits shown in Fig. 12. The saturation parameter S and its dependence on pressure are discussed in the text.

E. Pumping rate versus cell size

To compare the pumping rate for different size cells one must choose which optical-pumping parameter to keep constant. Maintaining our pragmatic orientation, we compare pumping rates for the same polarization ($\pm 1\%$) over the ranges shown in Figs. 6, 8, and 10. This is the most relevant approach, but also conservative because we observed that smaller cells could tolerate shorter relaxation times (hence, higher pumping rates) for the same polarization. We chose the discharge frequency and pumping transition that yielded the highest pumping rate for a given polarization.

We compare pumping rates for three different size cells with the following dimensions: 90 (4.7 cm i.d. by 5.4 cm long), 300 (4.7 cm i.d. by 17 cm long), and 600 cm^3 (7. 0 cm i.d. by 15 cm long). To test significantly larger cells would require an improved Helmholtz coil system in order to reduce relaxation from magnetic field gradients. In addition, as space constraints are often an issue for experiments at accelerators, we were interested in testing relatively small cells. For the 4.7-cm-i.d. cells the laser beam area was 12 cm^2, while for the 7.0-cm-i.d. cells it was 26 cm^2. In principle, comparing the 90- and 300-cm^3 cells, which differ only in their length, would isolate the effect of greater absorption of laser light, while comparing the 300- and 600-cm^3 cells, which differ mainly in their diameter, would isolate the effect of reduced saturation of the pumping transition (Sec. III D). However, because the size of the cell affects considerations such as the metastable lifetime, discharge characteristics, radiation trapping, etc., this may be at best a first-order analysis.

At 0.3 torr the ratios of the pumping rate were 1:3.6:4 for the three cells, increasing in volume. The pumping rate ratio for the 300-cm^3 cell as compared to the 90-cm^3 cell is actually somewhat larger than the increase in volume.

At 1.0 torr the ratios were 1:1.6–2.7:2.0, where the 1.6 and 2.7 correspond to weak and strong discharges, respectively. The improvement with cell size is roughly half that obtained at 0.3 torr. The 600-cm^3 cell is preferable for weak discharges, while the 300-cm^3 cell is preferable for strong discharges. For example, a pumping rate of 1.0×10^{19} (7×10^{18}) atoms/s with 50% polarization was obtained using the 300- (600-) cm^3 cell.

At 2.0 torr the ratios were 1:1.6–2.3:2.4–1.7, once again showing results for weak and strong discharges, respectively. Except for a difference in the behavior of the 600-cm^3 cell with respect to the discharge intensity, the results are similar to that obtained at 1.0 torr.

The results are provided mainly as documentation of our measurements. However, we make the following general observations: While the increase in the pumping rate was proportional to the cell length (or even a little better) at 0.3 torr, this is not generally the case at 1.0 and 2.0 torr. Possible reasons for the superior performance at 0.3 torr are weak absorption of the pumping light, insensitivity of the pumping rate to decreased laser intensity from whatever absorption is present (Sec. III D), and low sensitivity of the polarization to the discharge intensity. Measurements of the absorption and the metastable density would facilitate confirmation of these hypotheses. Although saturation is most relevant at low pressure (Sec. III D), only a small improvement was obtained at 0.3 torr by increasing the cell diameter.

IV. PROJECTIONS FOR TARGETS

In this section, we discuss what polarization we can expect to achieve in targets based on the results of Sec. III. Such projections are useful because comparison to actual target results can reveal experimental problems such as impurities in the ^{3}He gas.

The ideal conditions for the operation of internal and external targets are different. The most significant problem in the construction of dense external targets of polarized ^{3}He gas using the metastability exchange technique is that the optical pumping is efficient only for ^{3}He pressures of ~ 1 torr. In the Caltech target [13,19] this problem is addressed using a double cell system, in which the target cell is cooled to increase the ^{3}He density, while the optical pumping occurs in a room-temperature pumping cell. As the achievable density is limited by the minimum temperature that can be reached it is desirable to polarize at the highest pressure possible. Since the polarization declines with increasing pressure, a reasonable tradeoff of density and polarization is that pressure that maximizes the figure of merit P^2n, where P is the polarization and n is the target density. Although maximizing this figure of merit yields the minimum beam time to achieve a given statistical accuracy, the optimum choice will also depend upon the anticipated systematic errors and background levels. The figure of merit exhibits a broad maximum centered somewhat above 2 torr.

The internal target approach bypasses this density issue by trading density for average beam current to increase the luminosity of the target. Since the pressure in the target cell is much lower than in the pumping cell and is determined by the flow rate, we may choose whatever pumping cell pressure yields the best polarization for a given flow rate.

Using the data from 300-cm^3 cells shown in Figs. 6, 8, and 10 we now make projections for both internal targets and the external double cell cryogenic target. For the internal target the equilibrium polarization P is determined by setting the time derivative of NP to zero, where N is the number of atoms in the pumping cell and P is the polarization:

$$\frac{d}{dt}(NP)=N\frac{dP}{dt}+P\frac{dN}{dt}=0 \ . \tag{7}$$

From Eq. (3), $dP/dt=(P_0-P)/\tau(P)$, where P_0 is the polarization obtained in a sealed cell. We have replaced τ by $\tau(P)$ to allow for the dependence of the pumping rate on the polarization discussed in Sec. III B. Defining $R_p(P)\equiv NP_0/\tau(P)$ and $R_f\equiv dN/dt$, where R_f is the flow rate, we obtain

$$P=\frac{P_0}{1+[R_fP_0/R_p(P)]} \ , \tag{8}$$

where P_0 is the polarization in a sealed cell. For a given flow rate, Eq. (8) can be used to evaluate the equilibrium

polarization for any combination of the sealed cell parameters P_0 and $R_p(P)$. However, we need to evaluate the effective pumping rate $R_p(P)$, which is the pumping rate evaluated at the polarization P that will be maintained in the target, rather than the pumping rate R_p that is obtained from a fit to Eq. (3) (see Sec. III B). Typically the effect on the projections of using $R_p(P)$ rather than R_p is small (10%), so we make some simplifying approximations in the evaluation of $R_p(P)$. First, we use the linear approximation of $\tau_p^{-1}(P)$ shown in Fig. 3 for all our results, regardless of pressure and other conditions. We also set $\tau^{-1}(P)=\tau_p^{-1}(P)$ because typically $\tau_p \ll \tau_r$ [see Eq. (3b)]. Second, because $P \approx P_0$, we use $R_p(P_0)$ rather than $R_p(P)$, which yields a slightly conservative projection for P. Third, we set $R_p(P=0) \equiv R_p$, which slightly underestimates $R_p(P=0)$ and hence is also slightly conservative. With those approximations, $R_p(P)$ is given by

$$R_p(P_0)=R_p(1-0.94P_0) \ . \tag{9}$$

The current design flow rate for internal targets [14] is $R_f=1\times10^{17}$ atoms/s. From the 0.3- (1.0-) torr data we obtain a maximum projected polarization of $P=67\%$ (60%) for this flow rate, but under very different discharge conditions. At 0.3 torr, a strong discharge ($\tau_r=25$ s) is required to obtain a sufficient pumping rate ($R_p=2.2\times10^{18}$ atoms/s using C_8), but the polarization remains fairly high ($P_0=75\%$) at this high discharge intensity. At 1.0 torr a sufficient pumping rate is obtained with a weak discharge ($\tau_r=900$ s, $R_p \approx 1.5\times10^{18}$ atoms/s, and $P_0=68\%$), but any attempt at further improvement is thwarted by the rapid decrease in the polarization with increasing discharge intensity. Pressures of 0.3–0.5 torr may be the best regime for further improvements because of the relative insensitivity of the polarization to the discharge intensity and the rapid gain in the pumping rate with increasing cell size. In addition, operation at relatively short relaxation times may yield a system that is less sensitive to magnetic field gradients.

As the external cryogenic target has been described in detail elsewhere [13,19], we only consider aspects of this target that are important for a projection of the achievable polarization. The target consists of a Pyrex pumping cell, wherein the optical pumping occurs, connected by a transfer tube to a copper target cell. The target cell polarization P_t can be related to the pumping cell polarization P_p by solving the differential equations governing the diffusive transfer of polarized atoms between the two cells [5,13]. The relationship depends only on the average residence time in the target cell, t_t, and the relaxation time τ_t in the target cell:

$$\frac{P_t}{P_p}=\frac{1}{1+(t_t/\tau_t)} \ . \tag{10}$$

The pumping cell polarization can be related to the polarization achievable in a sealed cell by the following expression [13]:

$$P_p=\frac{P_0}{1+[P_t R_r/P_p R_p(P)]} \ , \tag{11}$$

where P_0 is the achievable polarization in a sealed cell, $R_r \equiv N_t P_0/\tau_t$, and N_t is the number of atoms in the target cell. This form is convenient because the ratio P_t/P_p is independent of the sealed cell parameters P_0 and $R_p(P)$.

To project a target polarization based on our sealed cell data, we need values for the residence time t_t, the number of atoms in the target cell, N_t, and the target relaxation time τ_t. For the Caltech target, $t_t=70$ s and $N_t=1.0\times10^{20}$ atoms (pressure of 2 torr at 15 K, target volume of 80 cm^3). The target relaxation time is obtained from measurements obtained during the recent experiment at the Bates linear accelerator and in an earlier test run [13]. Depolarization caused by wall collisions and the electron beam [13,31–33] are the major sources of relaxation in the target cell. The relaxation time with no beam depends upon the condition of the coating of frozen nitrogen on the target walls. The relaxation rate from the beam increases roughly linearly with the beam current. We consider two limits for our projection: $\tau_t=2000$ s, corresponding to the best wall coating and zero beam current, and $\tau_t=400$ s, the shortest relaxation time observed with a beam current of 40 μA. For $\tau_t=2000$ (400) s we obtain $R_r=0.5(2.5)\times10^{17}P_0$ atoms/s and $P_t/P_p=0.97$ (0.85). Using the 2-torr data and $\tau_t=2000$ s, we project $P_p=0.54$ and $P_t=0.52$ ($P_0=0.57$, $R_p=1.8\times10^{18}$ atoms/s). For $\tau_t=400$ s, we project $P_p=0.49$ and $P_t=0.42$ ($P_0=0.55$, $R_p=2.0\times10^{18}$ atoms/s). The ratio P_t/P_p could be improved by increasing the diameter of the transfer tube, which will decrease t_t. Hence we expect at least 42–52 % polarization in the target cell, at a density of 1.3×10^{18} atoms/cm^3.

V. CONCLUSION

In conclusion, the arc-lamp-pumped Nd:LMA laser has substantially improved the efficiency of optical pumping of ^{3}He by metastabilty exchange. We obtain 6 W of laser light at 1083 nm with a 1.5-GHz bandwidth. Under ideal conditions we have observed 85% polarization of ^{3}He nuclei. With pumping rates of 10^{18} atoms/s, we obtain 82% polarization, and at 10^{19} atoms/s, nearly 50% can be maintained.

We have measured the dependence of the effective pumping rate versus polarization that has been calculated by Larat [27]. Our studies show that the choice of frequency for the electrical discharge in the ^{3}He cell has a significant effect on the optical-pumping efficiency. We have also observed a pressure-dependent saturation of the increase of pumping rate with laser power.

The results of sealed cell data have been used to project performance for targets for nuclear physics experiments. Based on our data, we project that for the current internal target design flow rate of 1×10^{17} atoms/s, 67% polarization should be achievable, and future improvements are possible. For the Caltech double cell cryogenic target, we project at least 42% target polarization with a density of 1.3×10^{18} atoms/cm^3 for an electron beam current of 40 μA. This projected polarization is nearly a factor of 2 higher than was obtained in the first experi-

ment [11–13] using this target. The target is currently being tested using the developments discussed in this paper.

ACKNOWLEDGMENTS

We acknowledge the contributions of our colleagues, Wolfgang Lorenzon, Haiyan Gao, Cathleen Jones, and Robert Carr, and the technical contributions of Jim Pendlay, Al Massey, Jack Richards, and Gabor Faludi. We give special thanks for our interaction with Michele Leduc at L'Ecole Normale Supérieure and appreciate useful conversations with Laird Schearer, Padetha Tin, Kevin Lee, and Richard Milner. This work was supported by the National Science Foundation, Grant Nos. PHY88-17296 and PHY91-15574.

[1] F. D. Colegrove, L. D. Schearer, and G. K. Walters, Phys. Rev. **132**, 2561 (1963).
[2] C. G. Aminoff, C. Larat, M. Leduc, and F. Laloë, Rev. Phys. Appl. **24**, 827 (1989).
[3] C. L. Bohler *et al.*, J. Appl. Phys. **63**, 2497 (1988).
[4] J. M. Daniels, L. D. Schearer, M. Leduc, and P. J. Nacher, J. Opt. Soc. Am. B **4**, 1133 (1987).
[5] M. Leduc, S. B. Crampton, P. J. Nacher, and F. Laloë, Nucl. Sci. Appl. **2**, 1 (1984).
[6] C. G. Aminoff *et al.*, J. Lumin. **50**, 21 (1991).
[7] Padetha Tin and L. D. Schearer, J. Appl. Phys. **68**, 950 (1990).
[8] L. D. Schearer and Padetha Tin, J. Appl. Phys. **68**, 943 (1990).
[9] M. Leduc, J. Phys. (Paris) Colloq. **51**, C6-317 (1990).
[10] K. P. Coulter *et al.*, Nucl Instrum. Methods A **288**, 463 (1990).
[11] C. E. Woodward *et al.*, Phys. Rev. Lett. **65**, 698 (1990).
[12] C. E. Jones-Woodward *et al.*, Phys. Rev. C **44**, R571 (1991).
[13] Cathleen Jones, Ph.D. thesis, California Institute of Technology, 1991. Equation (11) can be obtained by manipulation of Eq. (D.62) of this reference and use of the definitions of $R_p(P)$ and R_r.
[14] R. Milner and K. Rith (unpublished).
[15] A. Bernstein, T. Chupp, R. McKeown, and R. Milner, Bates Proposal No. 88-25 (unpublished). Available from Bates Linear Accelerator Center, P.O. Box 846, Middleton, MA 01949.
[16] R. McKeown, CEBAF Proposal No. 89-007 (unpublished). Available from CEBAF, 12000 Jefferson Avenue, Newport News, VA 23606.
[17] G. Eckert *et al.*, Nucl. Instrum. Methods **320**, 53 (1992).
[18] E. W. Otten, Prog. Part. Nucl. Phys. **24**, 103 (1990).
[19] R. G. Milner, R. D. McKeown, and C. E. Woodward, Nucl. Instrum. Methods A **274**, 56 (1989).
[20] K. Lee, J. F. J. van den Brand, O. Hansen, and R. G. Milner, Nucl. Instrum. Methods (to be published).
[21] P. J. Nacher and M. Leduc, J. Phys. (Paris) **46**, 2057 (1985).
[22] F. Laloë, Ann. Phys. (Paris) **6**, 5 (1971).
[23] Milica Pavlovic and Franck Laloë, J. Phys. (Paris) **31**, 173 (1970).
[24] L. D. Schearer and G. K. Walters, Phys. Rev. **139**, A1398 (1965).
[25] Werner Heil and Laird Schearer (private communications).
[26] Comparison of pumping rates for different laser configurations is likely to depend on the optical-pumping conditions. We used a 4.7-cm-i.d. by 5.4-cm-long, 90-cm^3 cell at 0.8 torr, $\nu_d = 1.5$ MHz, $\tau_r = 20$ s, and $P_L = 1$ W for these tests. (The definitions of ν_d and τ_r can be found in Sec. III.) As compared to the results using two étalons, the pumping rate using a single 0.3-, 0.5- or 0.75-mm étalon was roughly 25% worse, and using a single 1.0-mm étalon was 60% worse. We note that the étalon(s) should be at normal incidence for a meaningful comparison.
[27] C. Larat, Ph.D. thesis, L'Ecole Normale Supérieure, 1991.
[28] M. Pinard and J. Van der Linde, Can. J. Phys. **52**, 1615 (1974).
[29] W. Lorenzon, T. R. Gentile, H. Gao, and R. D. McKeown, following paper, Phys. Rev. A **47**, 468 (1993).
[30] L. W. Anderson, F. M. Pipkin, and J. C. Baird, Jr., Phys. Rev. **120**, 1279 (1960).
[31] R. G. Milner, R. D. McKeown, and C. E. Woodward, Nucl. Instrum. Methods A **257**, 286 (1987).
[32] K. D. Bonin, T. G. Walker, and W. Happer, Phys. Rev. A **37**, 3270 (1988).
[33] K. D. Bonin, D. P. Saltzberg, and W. Happer, Phys. Rev. A **38**, 4481 (1988).